Journal of Geophysical Research: Space Physics

RESEARCH ARTICLE
10.1029/2018JA025182

First Ionospheric Results From the MAVEN Radio Occultation Science Experiment (ROSE)

Paul Withers[1,2], **M. Felici**[2], **M. Mendillo**[1,2], **L. Moore**[2], **C. Narvaez**[2], **M. F. Vogt**[2], **and B. M. Jakosky**[3]

[1]Department of Astronomy, Boston University, Boston, MA, USA, [2]Center for Space Physics, Boston University, Boston, MA, USA, [3]Laboratory for Atmospheric and Space Physics, University of Colorado Boulder, Boulder, CO, USA

Key Points:
- MAVEN now performs radio occultation observations
- Derived profiles consistent with previous experiments
- Observe full ionospheric profile with comprehensive MAVEN context

Correspondence to:
P. Withers,
withers@bu.edu

Citation:
Withers, P., Felici, M., Mendillo, M., Moore, L., Narvaez, C., Vogt, M. F., & Jakosky, B. M. (2018). First ionospheric results from the MAVEN Radio Occultation Science Experiment (ROSE). *Journal of Geophysical Research: Space Physics*, *123*. https://doi.org/10.1029/2018JA025182

Received 2 JAN 2018
Accepted 31 MAR 2018
Accepted article online 6 APR 2018

Abstract Radio occultation observations of the ionosphere of Mars can span the full vertical extent of the ionosphere, in contrast to in situ measurements that rarely sample the main region of the ionosphere. However, most existing radio occultation electron density profiles from Mars were acquired without clear context for the solar forcing or magnetospheric conditions, which presents challenges for the interpretation of these profiles. Here we present 48 ionospheric electron density profiles acquired by the Mars Atmosphere and Volatile EvolutioN mission (MAVEN) Radio Occultation Science Experiment (ROSE) from 5 July 2016 to 27 June 2017 at solar zenith angles of 54° to 101°. Latitude coverage is excellent, and comprehensive context for the interpretation of these profiles is provided by other MAVEN instruments. The profiles show a 9-km increase in ionospheric peak altitude in January 2017 that is associated with a lower atmospheric dust storm, variations in electron densities in the M1 layer that cannot be explained by variations in the solar soft X-ray flux, and topside electron densities that are larger in strongly magnetized regions than in weakly magnetized regions. MAVEN Radio Occultation Science Experiment electron density profiles are publicly available on the NASA Planetary Data System.

1. Introduction

Radio occultation measurements of ionospheric electron density profiles have been acquired at Mars by many previous spacecraft (Withers, 2010, and references therein). Orbiting spacecraft that have measured ionospheric electron density profiles using radio occultations include Mariner 9, Viking Orbiters 1 and 2, Mars Global Surveyor (MGS), and Mars Express. Mariner 9 acquired 114 profiles, 36 of which are from its extended mission and are of poor quality due to instrument degradation (Kliore et al., 1972, 1973; Withers, Weiner, & Ferreri, 2015). Viking Orbiters 1 and 2 acquired ~100 profiles (Kliore, 1992; Lindal et al., 1979; Zhang et al., 1990). MGS acquired 5,600 profiles, about 80% of the total acquired by all spacecraft (Hinson, 2007; Hinson et al., 1999; Mendillo et al., 2003; Withers et al., 2008). At the time of writing, Mars Express has observed approximately 1,000 profiles (Pätzold et al., 2016). Here we report on the Mars Atmosphere and Volatile EvolutioN mission (MAVEN) spacecraft's first radio occultation observations of Mars ionospheric electron density profiles.

MAVEN entered orbit around Mars in September 2014. Its science orbit has an inclination of 75°, a period of 4.5 hr, periapsis altitude of 140–170 km, and apoapsis altitude of ~6,200 km (Jakosky et al., 2015). MAVEN's "science objectives are to explore the interactions of the Sun and the solar wind with the Mars magnetosphere and upper atmosphere, to determine the structure of the upper atmosphere and ionosphere and the processes controlling it, to determine the escape rates from the upper atmosphere to space at the present epoch, and to measure properties that allow us to extrapolate these escape rates into the past to determine the total loss of atmospheric gas to space through time. These results will allow us to determine the importance of loss to space in changing the Mars climate and atmosphere through time, thereby providing important boundary conditions on the history of the habitability of Mars" (Jakosky et al., 2015). MAVEN's scientific payload measures "the energy and particle input from the Sun into the Mars upper atmosphere, the response of the upper atmosphere to that input, and the resulting escape of gas to space" (Jakosky et al., 2015).

The MAVEN Radio Occultation Science Experiment (ROSE) is a recent addition to MAVEN's suite of scientific investigations that uses the spacecraft's existing radio communications system. It conducted several test observations in February 2016 and began regular operations in July 2016. MAVEN ROSE measures vertical profiles of electron density in the ionosphere of Mars in order to (1) determine the vertical structure of plasma

in the ionosphere and (2) identify the density, altitude, and width of the ionospheric density peak. MAVEN ROSE contributes to the first high-level MAVEN science objective "Measure the composition and structure of the upper atmosphere and ionosphere today, and determine the processes responsible for controlling them" (Jakosky et al., 2015). In terms of the three areas listed above for the measurements made by MAVEN's scientific payload, MAVEN ROSE is aligned with the second, "the response of the upper atmosphere to [solar inputs]."

MAVEN ROSE electron density measurements are obtained from two-way, X-band (7–8 GHz) radio occultations of the ionosphere of Mars. MAVEN ROSE measurements are acquired when the Earth-Mars-MAVEN geometry is such that the radio signal between Earth and MAVEN passes through the ionosphere and atmosphere of Mars. These occultation opportunities occur at most twice per 4.5 hr orbit. Due to the precession of MAVEN's orbital plane and the orbital motion of Earth and Mars around the Sun, occultation opportunities occur in seasons a few months in duration that are separated by intervals of similar duration. Unlike many recent Mars orbiters, MAVEN does not have a Sun-synchronous orbit and its orbital plane precesses relatively rapidly. It takes approximately 6 months for the local true solar time of periapsis to move through a complete day (S. Demcak, personal communication, March 15, 2018; Jakosky et al., 2015). Consequently, the solar zenith angle of MAVEN occultations also changes relatively rapidly.

Raw MAVEN ROSE data from 48 ingress occultations conducted from 5 July 2016 to 27 June 2017 have been processed to yield electron density profiles. The raw data, intermediate products, and electron density profiles have been archived on the Planetary Plasma Interactions node of the NASA Planetary Data System. Data from the corresponding egress occultations have not yet been processed to yield reliable electron density profiles. The aims of this article are to discuss the key characteristics of the 48 archived electron density profiles and to report the first scientific results obtained from analysis of them.

Section 2 outlines the method used to conduct and process these radio occultation observations. Section 3 uses a single electron density profile to illustrate the vertical coverage and data quality of the MAVEN ROSE profiles. Section 4 demonstrates the validity of the MAVEN ROSE electron density profiles. Section 5 reports the results of initial investigations into the effects of lower atmospheric dust storms, variations in solar irradiance, and magnetic field conditions on MAVEN ROSE electron density profiles. Section 6 states the conclusions of this work.

2. Observational Method

MAVEN ROSE generally conducts two-way radio occultations at X-band (7-GHz uplink from Earth to MAVEN then 8-GHz downlink from MAVEN to Earth). During a MAVEN ROSE occultation observation, the radio signal received on Earth is recorded by dedicated radio science receivers at the NASA Deep Space Network sites. The JPL Radio Science Systems Group (RSSG) uses these data to generate time series of the observed frequency of the received radio signal. Due to refraction in the ionosphere and atmosphere of Mars, the path of a radio signal is slightly bent. This affects the Doppler shift experienced by the radio signal. As a result, the observed frequency differs from the frequency predicted based on the known motions of the transmitting and receiving antennas (Withers et al., 2014, and references therein). The Radio Science Systems Group determines time series of these frequency differences, from which Boston University determines vertical profiles of electron density in the ionosphere of Mars.

The general principles of how electron density profiles are generated from radio occultation observations were first published decades ago (e.g., Fjeldbo et al., 1971). A description of the data processing is available in the MAVEN ROSE Planetary Data System documentation, and a dedicated manuscript on this topic is currently in preparation. Here we briefly summarize key aspects of the current data processing method. The specific implementation for MAVEN ROSE of the long-established general principles follows equations (A1)–(A3) of Jenkins et al. (1994). One additional relationship is required to close this set of equations. Since the ionosphere is the primary focus of these MAVEN observations, we assume that all refraction is caused by plasma and neglect refraction by the neutral atmosphere. As discussed in more detail in section 3, this assumption is valid at altitudes above approximately 90-km altitude. Throughout the ionosphere, plasma refractivity is orders of magnitude greater than neutral refractivity (Withers, 2010). This assumption is sufficient to provide the required final relationship. Specifically, the ratio of the total bending angle of the uplink ray to the total bending angle of the downlink ray is equal to the square of the turn-around ratio (Withers, 2010). The terms "bending angle," "uplink ray," and "downlink ray" are defined in earlier detailed descriptions of radio occultation experiments (e.g., Withers, 2010, and references therein). The turn-around ratio, which is the ratio of the

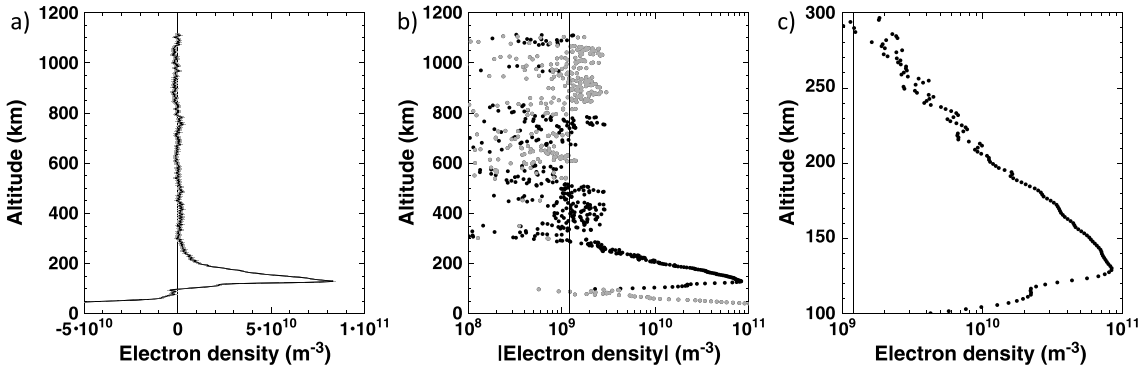

Figure 1. (a) Mars Atmosphere and Volatile EvolutioN mission Radio Occultation Science Experiment (MAVEN ROSE) electron density profile from 24 January 2017 at a solar zenith angle of 75°. Gray-shaded region indicates 1-σ uncertainties in electron density. Vertical line indicates zero. As discussed in the text, large negative densities at low altitudes are not reliable. (b) The same MAVEN ROSE electron density profile as in panel (a) but shown with a logarithmic density axis. The magnitude of the electron density is shown. Positive densities are shown by black symbols, and negative densities are shown by gray symbols. The vertical line indicates the measurement uncertainty of 1.2×10^9 m^{-3}. As discussed in the text, large negative densities at low altitudes are not reliable. (c) As panel (b) but zoomed in to highlight the main regions of the ionosphere.

frequency transmitted by MAVEN to the frequency received by MAVEN, is 880/749. The current data processing method does not yield neutral atmospheric profiles, although improved methods could generate them from the archived raw data from the surface to approximately 50-km altitude (Withers et al., 2014).

3. Example Electron Density Profile

Figure 1 shows a MAVEN ROSE electron density profile from 24 January 2017 at a solar zenith angle of 75°. In this example, the electron density profile extends to 1,100-km altitude with a measurement uncertainty of 1.2×10^9 m^{-3}. However, electron densities above 300-km altitude are not significant relative to the uncertainty in this example. The same electron density uncertainty is assigned to all measurements in a given profile. This is derived from electron densities at high altitudes, where ionospheric plasma densities are small and measured densities are dominated by noise. The uncertainty for a given profile is calculated as the root-mean square of all electron density values measured above 400 km in that profile. Between 100- and 300-km altitude, the electron density profile is similar to those reported by previous radio occultation experiments (Withers, 2009, and references therein). In this profile, electron densities in the topside ionosphere decrease exponentially with increasing altitude. The main ionospheric peak (the M2 layer) occurs near 130-km altitude. Below it, a shoulder (the M1 layer) occurs near 115-km altitude. Below the M1 layer, electron densities decrease rapidly with decreasing altitude and reach the measurement uncertainty at 100-km altitude. Below 90 km, reported electron densities are negative and their magnitudes exceed the measurement uncertainty: clearly, these values are not realistic. Here refraction of the radio signal is dominated by the neutral atmosphere, which is neglected in the plasma-focused data processing method outlined in section 2. These values should be ignored by data users.

4. Validation of Dataset

Figure 2 shows an example of the validation of the MAVEN ROSE profiles. It shows a MAVEN ROSE electron density profile from 17 January 2017 at a solar zenith angle of 80° (black line). It also shows nine MGS profiles (gray lines) from 1 May 2005 and the two Mariner 9 profiles from orbits 376 and 378 (red lines), all of which are at solar zenith angle between 79° and 81°. In the topside ionosphere, the MAVEN ROSE profile is consistent with the earlier profiles. The altitude and shape of the M2 layer and the altitude of the M1 layer are also consistent. However, the electron density at the M2 layer in the MAVEN ROSE profile (6.5×10^{10} m^{-3}) is smaller than the comparable electron densities in the earlier profiles. It is visibly less than the two Mariner 9 peak densities (7.8 and 9.1×10^{10} m^{-3}). Also, it is slightly less than the mean value of this set of nine MGS peak densities, 7.0×10^{10} m^{-3}. Moreover, the electron density in the M1 layer in the MAVEN ROSE profile is much smaller than the comparable electron densities in the earlier profiles. In an analysis of MGS profiles, Fallows et al. (2015a) found that, at 80° solar zenith angle, the M1 layer occurred at 109 km and had a density of 3.0×10^{10} m^{-3}. In this MAVEN ROSE profile, the density at 109 km is less than half that — 1.4×10^{10} m^{-3}.

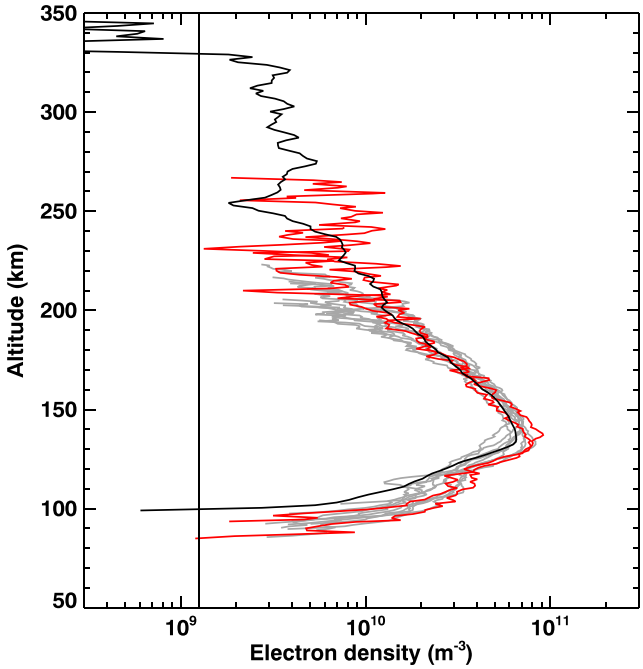

Figure 2. The black curve shows the Mars Atmosphere and Volatile EvolutioN mission Radio Occultation Science Experiment (MAVEN ROSE) electron density profile from 17 January 2017 at a solar zenith angle of 80°. The nine gray curves show a set of Mars Global Surveyor electron density profiles at similar solar zenith angles. The two red curves show Mariner 9 electron density profiles at similar solar zenith angles. The vertical line indicates the MAVEN ROSE measurement uncertainty of 1.3×10^9 m^{-3}.

We attribute these differences to the different responses of the M1 and M2 layers to variations in solar activity. The production of plasma in the M2 layer is driven by photoionization by solar extreme ultraviolet (EUV) photons in the 15- to 90-nm range, whereas the production of plasma in the M1 layer is driven by photoionization by solar soft X-ray photons in the 0- to 15-nm range (e.g., Fallows et al., 2015a, 2015b; Fox & Yeager, 2009; Girazian & Withers, 2015). The MAVEN ROSE profile was acquired at low solar activity, whereas the MGS and Mariner 9 profiles shown here were acquired at significantly higher solar activity. The monthly average of the *F*10.7 value at 1 AU was in the range of 70–90 units during periods when MAVEN ROSE observations were acquired but in the range of 100–150 units during periods when MGS and Mariner 9 observations were acquired (https://www.ngdc.noaa.gov/stp/space-weather/solar-data/solar-features/solar-radio/noontime-flux/penticton/penticton_adjusted/listings/listing_drao_noontime-flux-adjusted_monthly.txt). As solar activity increases, the solar EUV flux responsible for the M2 layer increases. The solar soft X-ray flux responsible for the M1 layer also increases. Yet the relative increase in flux is greater for the soft X-ray flux than for the EUV flux (i.e., the solar spectrum hardens with increasing solar activity; e.g., Fox & Yeager, 2009; Girazian et al., 2015). Hence, the MAVEN ROSE M1 and M2 peak densities are smaller than corresponding peak densities in the earlier profiles and the relative difference in peak densities is greater for the M1 layer than the M2 layer. This example demonstrates the validity of the MAVEN ROSE profiles. The profiles generally agree with similar observations by earlier experiments, and differences that do exist can be justified.

Figure 3 shows the dependence of maximum density, altitude of maximum electron density, and total electron content on solar zenith angle. The uncertainty in peak density is the measurement uncertainty in the electron density profile. The uncertainty in peak altitude was found using a Monte Carlo approach. For each observed profile, an ensemble of simulated profiles was generated in which each density value was replaced by a random number sampled from a normal distribution with mean equal to that density value and standard deviation equal to the measurement uncertainty. The altitude in peak electron density was found for each profile in the ensemble. The uncertainty in peak altitude was defined as the standard deviation of this set of peak altitudes. Total electron content is the integral of electron density with respect to altitude. Here we adopt an integration range of 80 to 270 km for consistency with recent studies using Mars Reconnaissance Orbiter (MRO) Shallow Radar (SHARAD) observations (Mendillo et al., 2017). The uncertainty in total electron content

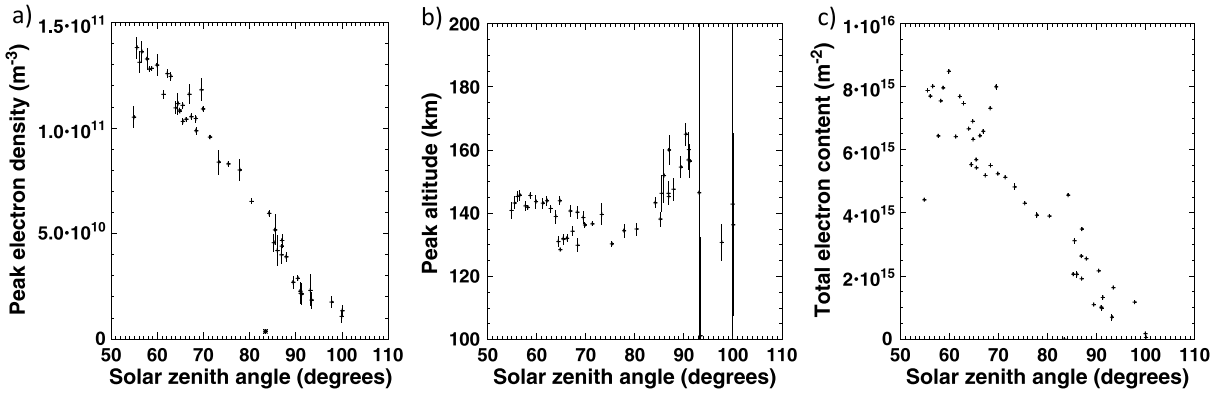

Figure 3. (a) Dependence of peak electron density on solar zenith angle. Measurement uncertainties are indicated by the vertical extent of the symbols. In some instances, measurement uncertainties are less than the symbol size. One measurement is shown by an asterisk. This is the unusually low peak density of 4×10^9 m^{-3} at a solar zenith angle of 83°. It is misleading because, due to a timing error, the observed profile covers only altitudes above 300 km and does not sample the main ionospheric region. (b) Dependence of peak altitude on solar zenith angle. Altitude uncertainties are indicated by the vertical extent of the symbols. In some instances, altitude uncertainties are less than the symbol size. At high solar zenith angles, altitude uncertainties can be very large due to the small peak densities. (c) Dependence of total electron content on solar zenith angle. Total electron content uncertainties are indicated by the vertical extent of the symbols. In many instances, these uncertainties are less than the symbol size.

was found using the same Monte Carlo approach as for peak altitude. In Figure 3, peak density decreases, peak altitude increases, and total electron content decreases as solar zenith angle increases. The increase in peak altitude occurs at solar zenith angles greater than 75°. These trends are expected for a photochemically controlled ionosphere (e.g., Withers, 2009, and references therein). Again, this example demonstrates the validity of the MAVEN ROSE profiles.

The characteristics of the MAVEN ROSE profiles can be compared to those of the widely used MGS profiles (Table 1). MGS profiles are numerous and closely spaced in time but have limited vertical coverage, latitude coverage, solar zenith angle coverage, and context. By contrast, MAVEN ROSE profiles are few and far apart in time but have comprehensive vertical coverage, latitude coverage, solar zenith angle coverage, and context. These two datasets can be considered complementary. For example, the MGS profiles are well suited to studies of how rare events perturb the ionosphere, while the MAVEN ROSE profiles are well suited to studies of how thermosphere, ionosphere, and magnetosphere are coupled during normal conditions.

Table 1
Comparison of MGS and MAVEN ROSE Electron Density Profiles

	MGS	MAVEN ROSE
Average topmost altitude	213 km	900 km[a]
Average uncertainty	4.6×10^9 m^{-3}	3.1×10^9 m^{-3}
Characteristic altitude resolution	~1 km	~1 km
Number of archived profiles	5,600	48
*F*10.7 range (1 AU)	90–180	70–90
Characteristic time interval	2 hr	3 days
Latitude coverage	60°N to 86°N (5,380) 70°S to 64°S (220)	84°S to 65°N[b]
SZA range	70°–90°	54°–101°
Complementary observations	Limited[c]	Comprehensive[d]

[a]The average altitude at which MAVEN ROSE electron densities first fall below their uncertainty when moving upward from the ionospheric peak is 288 km. [b]However, only two profiles are equatorward of 30° latitude. [c]MGS magnetometer and electron reflectometer observations at 400-km altitude and 2 a.m./2 p.m. local time. [d]MAVEN observations of the solar photon flux, solar particle flux, and magnetospheric conditions, plus near-simultaneous, but not collocated, in situ and remote sensing observations of ionospheric and thermospheric conditions. MGS = Mars Global Surveyor; MAVEN = Mars Atmosphere and Volatile EvolutioN mission; ROSE = Radio Occultation Science Experiment; SZA = solar zenith angle.

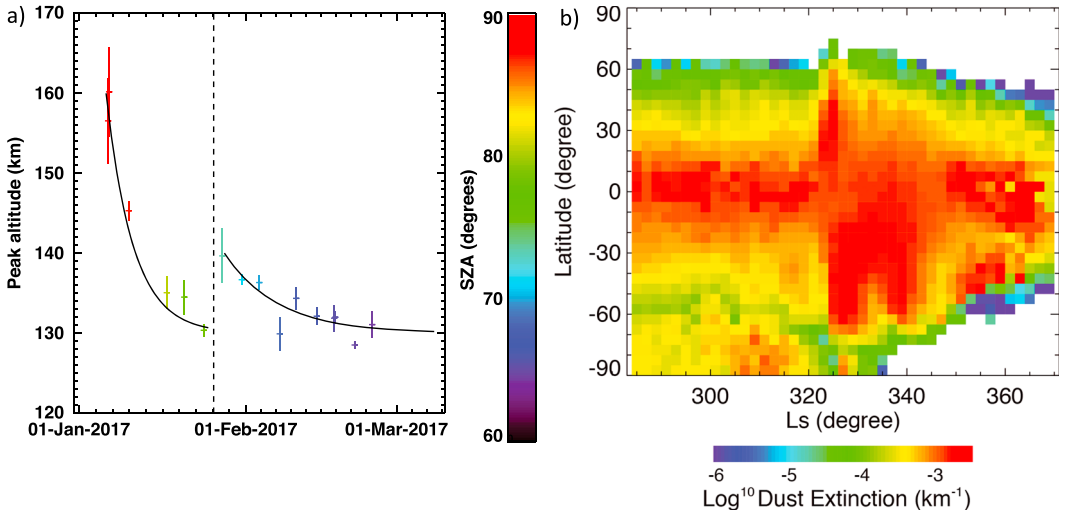

Figure 4. (a) Peak altitude as a function of time for the occultations in January–February 2017. Altitude uncertainties are indicated by the vertical extent of the symbols. Solar zenith angles are indicated by the color of the symbols. The vertical dashed line indicates the approximate start of the dust event. The two solid lines are illustrative representations of trends in the data—they are not fits. At early dates, peak altitude z is represented by $z = 130\ \text{km} + 30\ \text{km}\ \exp\left(-t_1/5\ \text{days}\right)$ where t_1 is time since 6 January 2017. At later dates, peak altitude z is represented by $z = 130\ \text{km} + 10\ \text{km}\ \exp\left(-t_2/10\ \text{days}\right)$ where t_2 is time since 28 January 2017. (b) Dust extinction at 50 Pa (~25-km altitude) from 20 December 2016 ($Ls = 283°$) to 30 May 2017 ($Ls = 12°$) as measured by the Mars Climate Sounder instrument (McCleese et al., 2007).

5. Case Studies

Here we present results from several focused scientific investigations that use the MAVEN ROSE profiles. These investigations consider the ionospheric response to dust storms in the lower atmosphere (section 5.1), solar soft X-ray irradiance (section 5.2), and crustal magnetic field conditions (section 5.3).

5.1. Dust Storms in the Lower Atmosphere

Figure 4a shows peak altitude as a function of time for the occultations in January–February 2017. The general trend of peak altitude decreasing as time increases is caused by solar zenith angle decreasing as time increases (Withers, 2009, and references therein). However, two distinct trends are present. The first trend applies to observations on and before 24 January 2017, and the second trend applies to observations on and after 28 January 2017. A discontinuity is apparent between these two trends as the peak altitude on 28 January 2017 (73° solar zenith angle, 52°N) is 9 km greater than on 24 January 2017 (75° SZA, 54°N). This behavior is illustrated by the lines shown in Figure 4a.

This is an example of the ionospheric peak altitude increasing in response to a dust storm in the lower atmosphere, as previously seen by, e.g., Kliore et al. (1972), Hantsch and Bauer (1990), and Withers and Pratt (2013). Figure 4b shows how the meridional structure of lower atmospheric dust extinction varies with time. A dust event occurs in the Southern Hemisphere on roughly 20 January 2017 ($Ls = 305°$) and persists until the end of this occultation season. Although changes in the zonally averaged atmospheric dust extinction are restricted to latitudes poleward of 60°S, the ionosphere at 52°N responds within a few days despite the thousands of kilometers separation. Such rapid thermospheric and ionospheric responses are consistent with previous observations (e.g., Keating et al., 1998; Withers & Pratt, 2013). Other MAVEN instruments also observed changes in thermospheric conditions during this dust event. Liu et al. (2018) reported significant increases in the NGIMS Ar density at 180 and 200 km at 30°S latitude (their episode 1).

5.2. Solar Soft X-Ray Irradiance

Figure 5 shows profiles from 9 August 2016 (70° solar zenith angle) and 16 August 2016 (67° solar zenith angle). Their M2 peak densities, M2 peak altitudes, and M1 peak altitudes are similar. However, their M1 peak densities are not similar. The measured electron density at 110–120 km is $\sim 3 \times 10^{10}\ \text{m}^{-3}$ on 9 August 2016 but $\sim 5 \times 10^{10}\ \text{m}^{-3}$ on 16 August 2016.

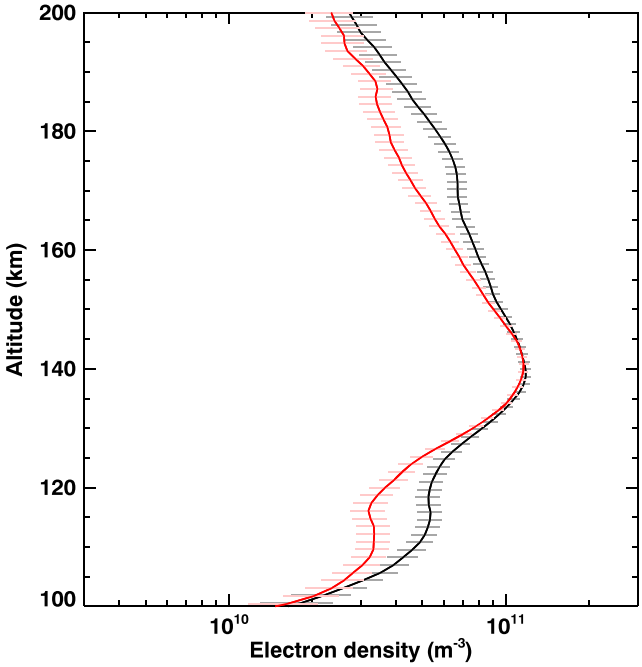

Figure 5. Mars Atmosphere and Volatile Evolution Mission Radio Occultation Science Experiment electron density profiles from 9 August 2016 (70° solar zenith angle, red curve) and 16 August 2016 (67° solar zenith angle, black curve). Horizontal lines indicate 1-σ uncertainties in electron density.

In simple photochemical theory, electron density is proportional to the square root of the ionizing flux (Schunk & Nagy, 2009; Withers, 2009) such that an increase in electron density by a factor of 1.7 implies an increase in ionizing flux by a factor of 2.8 from 9 August 2016 to 16 August 2016. Previous workers have concluded that photons in the 0- to 15-nm range contribute to ionization in the M1 layer (e.g., Fallows et al., 2015a, 2015b, and references therein). Yet observations by the MAVEN EUVM instrument (Eparvier et al., 2015) show that the 0.1- to 7-nm flux decreased by approximately 10% from 9 August 2016 to 16 August 2016 (E. Thiemann, personal communication, January 18, 2018). The longer wavelength 17- to 22-nm (ionizing EUV) and 121.6-nm (nonionizing Lyman-α) fluxes also decreased by similar amounts.

Therefore, variations in solar irradiance are not responsible for the 70% difference between the M1 peak densities observed on 9 August 2016 and 16 August 2016. Other factors must be responsible. A possible explanation is a change in the chemical composition of the neutral atmosphere, which would affect the composition of

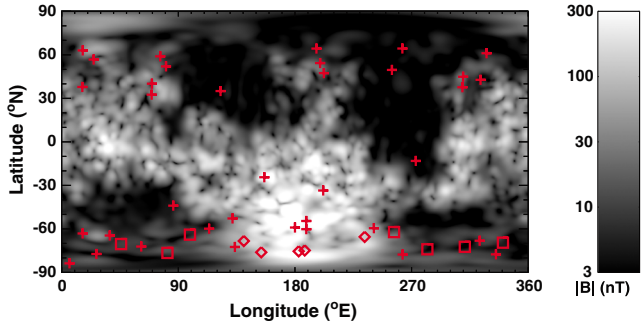

Figure 6. Locations of the Mars Atmosphere and Volatile Evolution Mission Radio Occultation Science Experiment electron density profiles. Diamonds indicate the locations of the five strongly magnetized profiles of section 5.3, and squares indicate the locations of the seven weakly magnetized profiles of section 5.3. Crosses indicate the locations of all other profiles. The background shading indicates the crustal magnetic field strength at 185 km predicted by the model of Morschhauser et al. (2014).

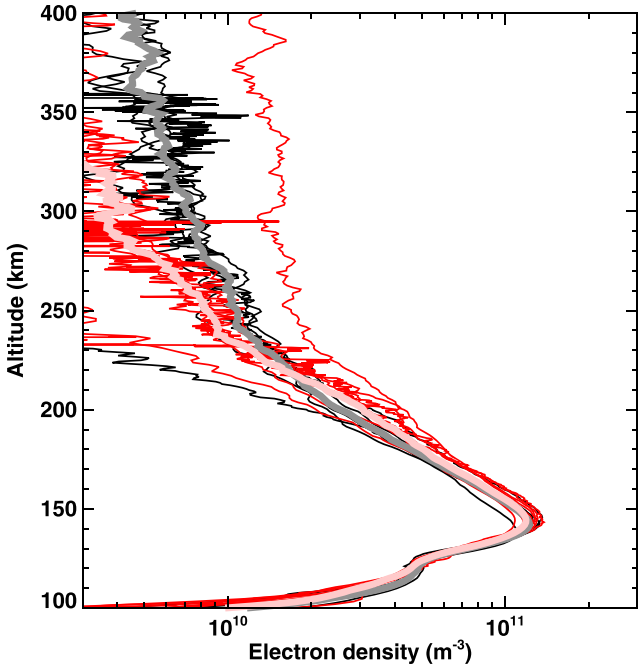

Figure 7. Black curves show five Mars Atmosphere and Volatile EvolutioN mission Radio Occultation Science Experiment (MAVEN ROSE) electron density profiles from strongly magnetized regions. Red curves show seven MAVEN ROSE electron density profiles from weakly magnetized regions. The thick gray line is the weighted mean of the five strong profiles, and the thick pink line is the weighted mean of the seven weak profiles.

ionospheric plasma and hence the plasma lifetime. In this scenario, plasma in the M1 region has a longer lifetime on 16 August 2016 than on 9 August 2016 because it contains a higher proportion of longer-lived ion species, such as NO^+ (Fox, 2004).

5.3. Crustal Magnetic Fields

Figure 6 shows that the MAVEN ROSE profiles are well distributed in latitude and longitude. As 10 of the 48 profiles are in regions where the modeled crustal magnetic field strength at 185 km exceeds 80 nT (Morschhauser et al., 2014), this dataset is well suited to studies of the ionospheric effects of crustal magnetic fields.

Figure 7 compares profiles acquired from strongly and weakly magnetized regions at similar dates, latitudes, and solar zenith angles. All profiles were acquired at August–October 2016, latitudes between 80°S and 60°S and solar zenith angles between 55° and 65°. The modeled crustal magnetic field strength at 185 km is greater than 80 nT for five strongly magnetized profiles (black lines) and is less than 20 nT for seven weakly magnetized profiles (red lines). This figure also shows the weighted means of the five strongly magnetized profiles (gray line) and the seven weakly magnetized profiles (pink line). The average strongly and weakly magnetized profiles are similar below 220 km. At higher altitudes, they are not. Average density is greater for strongly magnetized profiles than weakly magnetized profiles. It follows that the plasma scale height must also be greater in strongly magnetized regions than in weakly magnetized regions above 220 km.

This dependence of topside density on magnetic field strength is consistent with earlier work. In an analysis of the effects of crustal magnetic fields on ionospheric electron densities measured by the in situ MAVEN LPW instrument (Andersson et al., 2015), Flynn et al. (2017) found that densities at 200–400 km were 30% greater in strongly magnetized regions than in weakly magnetized regions.

6. Conclusions

The MAVEN ROSE investigation has successfully generated a set of 48 electron density profiles from the ionosphere of Mars. Comparison of these profiles to profiles from earlier missions, augmented by comparison of trends in peak electron density, peak altitude, and total electron content to results from other datasets, demonstrates that the profiles are reliable. The MAVEN ROSE profiles have comprehensive coverage in altitude, latitude, and solar zenith angle. Their measurement uncertainties are comparable to those of previous

radio occultation experiments. These profiles were acquired under low solar activities not sampled by the MGS radio occultation profiles (Withers, Morgan, & Gurnett, 2015). These profiles show an increase in peak altitude during a lower atmospheric dust storm, variations in M1 layer densities that are not caused by variations in the solar soft X-ray flux, and enhanced topside electron densities in strongly magnetized regions.

Typically, two ingress and two egress occultations are observed by MAVEN ROSE each week. Although MAVEN ROSE profiles are acquired infrequently by comparison with the standard set by MGS, their value is enhanced by the availability of simultaneous observations of the solar photon flux, solar particle flux, and magnetospheric and ionospheric conditions by other MAVEN instruments and by instruments on other active Mars spacecraft. MAVEN ROSE electron density profiles are publicly available on the NASA Planetary Data System.

Acknowledgments
We acknowledge Wayne Sidney, Mike Haggard, and other colleagues at Lockheed Martin for implementing MAVEN ROSE spacecraft operations; Kamal Oudrhiri, Danny Kahan, and other colleagues at the JPL RSSG and DSN for implementing MAVEN ROSE ground operations; and Dick Simpson for supporting archiving. We thank G. Liu (University of California Berkeley) for providing Figure 4b, M. Grandin for a helpful review, and R. Lillis (University of California Berkeley) for a helpful review and a magnetic field model. The MAVEN project is supported by NASA through the Mars Exploration Program. MAVEN data are available from the PPI node of the NASA Planetary Data System (https://pds-ppi.igpp.ucla.edu/mission/MAVEN/MAVEN/ROSE).

References

Andersson, L., Ergun, R. E., Delory, G. T., Eriksson, A., Westfall, J., Reed, H., et al. (2015). The Langmuir Probe and Waves (LPW) instrument for MAVEN. *Space Science Reviews*, *195*, 173–198. https://doi.org/10.1007/s11214-015-0194-3

Eparvier, F. G., Chamberlin, P. C., Woods, T. N., & Thiemann, E. M. B. (2015). The solar Extreme Ultraviolet Monitor for MAVEN. *Space Science Reviews*, *195*, 293–301. https://doi.org/10.1007/s11214-015-0195-2

Fallows, K., Withers, P., & Matta, M. (2015a). An observational study of the influence of solar zenith angle on properties of the M1 layer of the Mars ionosphere. *Journal of Geophysical Research: Space Physics*, *120*, 1299–1310. https://doi.org/10.1002/2014JA020750

Fallows, K., Withers, P., & Matta, M. (2015b). Numerical simulations of the influence of solar zenith angle on properties of the M1 layer of the Mars ionosphere. *Journal of Geophysical Research: Space Physics*, *120*, 6707–6721. https://doi.org/10.1002/2014JA020947

Fjeldbo, G., Kliore, A. J., & Eshleman, V. R. (1971). The neutral atmosphere of Venus as studied with the Mariner V radio occultation experiments. *The Astronomical Journal*, *76*, 123–140.

Flynn, C. L., Vogt, M. F., Withers, P., Andersson, L., England, S., & Liu, G. (2017). MAVEN observations of the effects of crustal magnetic fields on electron density and temperature in the Martian dayside ionosphere. *Geophysical Research Letters*, *44*, 10,812–10,821. https://doi.org/10.1002/2017GL075367

Fox, J. L. (2004). Response of the Martian thermosphere/ionosphere to enhanced fluxes of solar soft X rays. *Journal of Geophysical Research*, *109*, A11310. https://doi.org/10.1029/2004JA010380

Fox, J. L., & Yeager, K. E. (2009). MGS electron density profiles: Analysis of the peak magnitudes. *Icarus*, *200*, 468–479. https://doi.org/10.1016/j.icarus.2008.12.002

Girazian, Z., & Withers, P. (2015). An empirical model of the extreme ultraviolet solar spectrum as a function of $F_{10.7}$ based on TIMED-SEE data. *Journal of Geophysical Research: Space Physics*, *120*, 6779–6794. https://doi.org/10.1002/2015JA021436

Girazian, Z., Withers, P., Häusler, B., Pätzold, M., Tellmann, S., & Peter, K. (2015). Characterization of the lower layer in the dayside Venus ionosphere and comparisons with Mars. *Planetary and Space Science*, *117*, 146–158. https://doi.org/10.1016/j.pss.2015.06.007

Hantsch, M. H., & Bauer, S. J. (1990). Solar control of the Mars ionosphere. *Planetary and Space Science*, *38*, 539–542.

Hinson, D. P. (2007). MGS RST science data products, USA_NASA_JPL_MORS_1102. In R. A. Simpson (Ed.), *MGS-M-RSS-5-EDS-V1.0*. NASA Planetary Data System.

Hinson, D. P., Simpson, R. A., Twicken, J. D., Tyler, G. L., & Flasar, F. M. (1999). Initial results from radio occultation measurements with Mars Global Surveyor. *Journal of Geophysical Research*, *104*, 26,997–27,012.

Jakosky, B. M., Lin, R. P., Grebowsky, J. M., Luhmann, J. G., Mitchell, D. F., Beutelschies, G., et al. (2015). The Mars Atmosphere and Volatile Evolution (MAVEN) Mission. *Space Science Reviews*, *195*, 3–48. https://doi.org/10.1007/s11214-015-0139-x

Jenkins, J. M., Steffes, P. G., Hinson, D. P., Twicken, J. D., & Tyler, G. L. (1994). Radio occultation studies of the Venus atmosphere with the Magellan spacecraft. 2: Results from the October 1991 experiments. *Icarus*, *110*, 79–94. https://doi.org/10.1006/icar.1994.1108

Keating, G. M., Bougher, S. W., Zurek, R. W., Tolson, R. H., Cancro, G. J., Noll, S. N., et al. (1998). The structure of the upper atmosphere of Mars: In situ accelerometer measurements from Mars Global Surveyor. *Science*, *279*, 1672–1676.

Kliore, A. J. (1992). Radio occultation observations of the ionospheres of Mars and Venus, *Venus and Mars: Atmospheres, ionospheres, and solar wind interactions, Geophysical Monograph Series* (Vol. 66, pp. 265–276). Washington, DC: American Geophysical Union.

Kliore, A. J., Cain, D. L., Fjeldbo, G., Seidel, B. L., Sykes, M. J., & Rasool, S. I. (1972). The atmosphere of Mars from Mariner 9 radio occultation measurements. *Icarus*, *17*, 484–516.

Kliore, A. J., Fjeldbo, G., Seidel, B. L., Sykes, M. J., & Woiceshyn, P. M. (1973). *S* band radio occultation measurements of the atmosphere and topography of Mars with Mariner 9: Extended mission coverage of polar and intermediate latitudes. *Journal of Geophysical Research*, *78*, 4331–4351. https://doi.org/10.1029/JB078i020p04331

Lindal, G. F., Hotz, H. B., Sweetnam, D. N., Shippony, Z., Brenkle, J. P., Hartsell, G. V., & Spear, R. T. (1979). Viking radio occultation measurements of the atmosphere and topography of Mars—Data acquired during 1 Martian year of tracking. *Journal of Geophysical Research*, *84*, 8443–8456. https://doi.org/10.1029/JB084iB14p08443

Liu, G., England, S. L., Lillis, R. J., Withers, P., Mahaffy, P. R., Rowland, D. E., et al. (2018). Thermospheric expansion associated with dust increase in the lower atmosphere on Mars observed by MAVEN/NGIMS. *Geophysical Research Letters*, *45*, 2901–2910. https://doi.org/doi:10.1002/2018GL077525

McCleese, D. J., Schofield, J. T., Taylor, F. W., Calcutt, S. B., Foote, M. C., Kass, D. M., et al. (2007). Mars Climate Sounder: An investigation of thermal and water vapor structure, dust and condensate distributions in the atmosphere, and energy balance of the polar regions. *Journal of Geophysical Research*, *112*, E05S06. https://doi.org/10.1029/2006JE002790

Mendillo, M., Smith, S., Wroten, J., Rishbeth, H., & Hinson, D. (2003). Simultaneous ionospheric variability on Earth and Mars. *Journal of Geophysical Research*, *108*, 1432. https://doi.org/10.1029/2003JA009961

Mendillo, M., Narvaez, C., & Campbell, B. (2017). The total electron content of the Martian ionosphere from MRO/SHARAD observations. *Journal of Geophysical Research: Planets*, *122*, 2182–2192. https://doi.org/10.1002/2017JE005391

Morschhauser, A., Lesur, V., & Grott, M. (2014). A spherical harmonic model of the lithospheric magnetic field of Mars. *Journal of Geophysical Research: Planets*, *119*, 1162–1188. https://doi.org/10.1002/2013JE004555

Pätzold, M., Häusler, B., Tyler, G. L., Andert, T., Asmar, S. W., Bird, M. K., et al. (2016). Mars Express 10 years at Mars: Observations by the Mars Express Radio Science Experiment (MaRS). *Planetary and Space Science*, *127*, 44–90. https://doi.org/10.1016/j.pss.2016.02.013

Schunk, R. W., & Nagy, A. F. (2009). *Ionospheres* (2nd ed.). New York: Cambridge University Press.

Withers, P. (2009). A review of observed variability in the dayside ionosphere of Mars. *Advances in Space Research*, *44*, 277–307. https://doi.org/10.1016/j.asr.2009.04.027

Withers, P. (2010). Prediction of uncertainties in atmospheric properties measured by radio occultation experiments. *Advances in Space Research*, *46*, 58–73. https://doi.org/10.1016/j.asr.2010.03.004

Withers, P., & Pratt, R. (2013). An observational study of the response of the upper atmosphere of Mars to lower atmospheric dust storms. *Icarus*, *225*, 378–389. https://doi.org/10.1016/j.icarus.2013.02.032

Withers, P., Mendillo, M., Hinson, D. P., & Cahoy, K. (2008). Physical characteristics and occurrence rates of meteoric plasma layers detected in the Martian ionosphere by the Mars Global Surveyor Radio Science Experiment. *Journal of Geophysical Research*, *113*, A12314. https://doi.org/10.1029/2008JA013636

Withers, P., Moore, L., Cahoy, K., & Beerer, I. (2014). How to process radio occultation data: 1. From time series of frequency residuals to vertical profiles of atmospheric and ionospheric properties. *Planetary and Space Science*, *101*, 77–88. https://doi.org/10.1016/j.pss.2014.06.011

Withers, P., Weiner, S., & Ferreri, N. R. (2015). Recovery and validation of Mars ionospheric electron density profiles from Mariner 9. *Earth, Planets and Space*, *67*, 194. https://doi.org/10.1186/s40623-015-0364-2

Withers, P., Morgan, D. D., & Gurnett, D. A. (2015). Variations in peak electron densities in the ionosphere of Mars over a full solar cycle. *Icarus*, *251*, 5–11. https://doi.org/10.1016/j.icarus.2014.08.008

Zhang, M. H. G., Luhmann, J. G., Kliore, A. J., & Kim, J. (1990). A post-Pioneer Venus reassessment of the Martian dayside ionosphere as observed by radio occultation methods. *Journal of Geophysical Research*, *95*, 14,829–14,839.